Numerical simulation of micro-crack leakage on steam generator heat transfer tube

Zhao, X.; Liao, Y.; Wang, M.; Zhang, K.; Su, G. H.; Tian, W.; Qiu, S.; Lucas, D.;

Originally published:

August 2021

Nuclear Engineering and Design 382(2021), 111385

DOI: https://doi.org/10.1016/j.nucengdes.2021.111385

Perma-Link to Publication Repository of HZDR:

https://www.hzdr.de/publications/Publ-31731

Numerical simulation of micro-crack leakage on steam generator heat transfer tube

Xiaohan Zhao[1,2], Yixiang Liao[2]*, Mingjun Wang[1], Kui Zhang[1], G. H. Su[1]*, Wenxi Tian[1], Suizheng Qiu[1], Dirk Lucas[2]

y.liao@hzdr.de

ghsu@mail.xjtu.edu.cn

1 State Key Laboratory of Multiphase Flow in Power Engineering, School of Nuclear Science and Technology, Xi'an Jiaotong University

2 Helmholtz-Zentrum Dresden - Rossendorf, Institute of Fluid Dynamics, Bautzner Landstrasse 400, 01328 Dresden, Germany

Abstract

Flashing is frequently encountered in nuclear power systems for example as leakage occurring on the steam generator (SG) heat transfer tubes. Pressurized primary coolant flows rapidly through the crack and flashes into vapor. The pressure relief rate and loss rate of coolant, which affects largely the safety of fission reactors, are determined by the flashing phase change process. Information about the flashing phenomenon is of significance for the leakage online monitoring system, which ensures the normal operation of steam generator (SG) and safety of the reactor when tube rupture accidents occur. In this research, steady-state and transient 3D flashing flow inside a short micro-crack channel in the heat transfer tube wall of SG have been studied using FLUENT. The cavitation model and evaporation-condensation model, in combination with both the mixture two-phase flow and the Eulerian two-fluid model, are adopted to simulate the flashing phenomenon. The real geometry and operating conditions of AP1000 nuclear system are adopted to reflect the reality leakage phenomenon in SG. Two types of micro-crack shape including axial crack and circumferential crack, which both can happen in the reality, are considered. The CFD results gained from five different models have been compared with experimental data, and good agreement is demonstrated. The model comparison shows that the evaporation-condensation model behaves superior to the cavitation model in simulating the flashing phenomenon. Finally the leakage rates are gained under different crack shapes, sub-cooling degrees and backpressures with the most accuracy scheme. In addition, two-phase choking flow phenomenon is simulated by changing backpressure of cracked tubes. The simulation results in this research could be good reference for leakage prediction of micro-crack in SG to improve the operation performance of SG and safety of the whole nuclear power system.

Key words: micro-crack, SG, CFD, flash boiling, FLUENT

Nomenclature table	
Variable	Description
α	Volume of phase fraction
ρ	Density (kg/m^3)
v	Velocity (m/s)
m	Mass flow rate (kg/m^3)
m_{pq}^{+} m_{qp}^{+}	Positive mass flow rate per unit volume between phases (kg/m^3)
P	Pressure (Pa)
τ	Stress tensor
K_{pq}	Coefficient for phase interaction effect
F	Force on two-phase flow (Pa/m^2)
S_E	Energy source between phases in mixture model (W/m^3)
H	Enthalpy (kJ/kg)
H_{pi}, H_{qi}	Interfacial enthalpy (kJ/kg)
μ	Dynamic viscosity (N·s/㎡)
α_{nuc}	Nucleation site volume fraction (/m^3)
F_{vap}	Evaporation coefficient
R_b	Bubble radius (m)
F_{cond}	Condensation coefficient
Q	Energy source between two phases (J/m^3)
q	Energy source of phases and interfacial (J/m^3)
T	Temperature (K)
h	Heat transfer coefficient (W/(m^2·K))
A_i	Interfacial area (m^2)
d_b	Bubble diameter (m)
Pr	Prandtl number
Re	Reynolds number
Eo	Eötvös number
Nu	Nusselt number
C_D	Drag force coefficient
C_{vm}	Virtual mass force coefficient
C_{wl}	Wall lubrication force coefficient
$\vec{n}_w$	Vertical direction of wall
C_l	Lift force coefficient
Subscript	
p, q	*q* is a common phase and *p* is another phase in two fluid model
pq, qp	Effect between common phase with other phase in two fluid model
lift,q	Lift effect of a common phase in two fluid model
wl,q	Wall lubrication effect of a common phase in two fluid model

vm,q	Virtual mass effect of a common phase in two fluid model
td,q	Turbulent dispassion effect of a common phase in two fluid model
m	Mixture phase
v	Vapor phase
l	Liquid phase
k	Common phase in mixture model
eff	Effective coefficient
lv	Effect of liquid phase to vapor phase in mixture model
vl	Effect of vapor phase to liquid phase in mixture model
b	bubble
i	Interface of phases

Nomenclature table

Variable	Description
α	Volume of phase fraction
ρ	Density (kg/m^3)
v	Velocity (m/s)
m	Mass flow rate (kg/m^3)
m_{pq}^{+} m_{qp}^{+}	Positive mass flow rate per unit volume between phases (kg/m^3)
P	Pressure (Pa)
τ	Stress tensor
K_{pq}	Coefficient for phase interaction effect.
F	Force on two-phase flow (Pa/m^2)
S_E	Energy source between phases in mixture model (W/m^3)
H	Enthalpy (kJ/kg)
H_{pi}, H_{qi}	Interfacial enthalpy between bubble interface and two phases. (kJ/kg)
μ	Dynamic viscosity (N·s/㎡)
α_{nuc}	Nucleation site volume fraction (/m^3)
F_{vap}	Evaporation coefficient
R_b	Bubble radius (m)
F_{cond}	Condensation coefficient
Q	Energy source between two phases (J/m^3)
q	Energy source of phases and interfacial (J/m^3)
T	Temperature (K)
h	Heat transfer coefficient (W/(m^2·K))
A_i	Interfacial area (m^2)
d_b	Bubble diameter (m)
Pr	Prandtl number
Re	Reynolds number
Eo	Eötvös number
Nu	Nusselt number
C_D	Drag force coefficient
C_{vm}	Virtual mass force coefficient

C_{wl}	Wall lubrication force coefficient
$\vec{n}_w$	Vertical direction of wall
C_l	Lift force coefficient
Subscript	
p, q	q is a common phase and p is another phase in two fluid model
pq, qp	Effect between common phase with other phase in two fluid model
lift,q	Lift effect of a common phase in two fluid model
wl,q	Wall lubrication effect of a common phase in two fluid model
vm,q	Virtual mass effect of a common phase in two fluid model
td,q	Turbulent dispassion effect of a common phase in two fluid model
m	Mixture phase
v	Vapor phase
l	Liquid phase
k	Common phase in mixture model
eff	Effective coefficient
lv	Effect of liquid phase to vapor phase in mixture model
vl	Effect of vapor phase to liquid phase in mixture model
b	bubble
i	Interfacial position between phases

1. Introduction

Flashing like cavitation is a typical phase change phenomenon occurring when liquid experiences pressure drop. It may be encountered in many industrial systems and occasions including the SG, pressurized vessels and pipelines in pressurized water reactors (PWRs). As we know, the two-phase choking flow rate which determines the pressure relief rate and coolant loss rate of the two pressurized circuits in PWRs is related closely with the flashing process. A reliable correlation for the determination of this maximum flow rate is not yet available. Therefore, the research on 3D flashing flows as well as two-phase critical flows are quite necessary for the safety analysis of nuclear power systems.

Heat transfer tubes of SG are the most vulnerable barrier in the PWR pressure boundary due to their thin (~1mm) wall and extremely harsh operating environment. Tube failure accidents occur frequently in SG, which are caused by various kinds of corrosion processes, and greatly affect the operation performance and lifetime of SG. Leakage rate of micro-crack at the early rupture stage is an effective parameter for judging whether the SG could be used continually with help of tube plugging operations. Accurate prediction of leakage rate and subsequent operations are meaningful for online-monitoring systems to ensure normal performance of SG and reduce economic loss caused by replacing SG. Therefore, the Leak Before Break (LBB) analysis is quite important for maintaining the operation stability of SG and safety of reactor. Flashing and choking are key points in the LBB calculations considering huge temperature difference and pressure drop between two sides of SG tubes. Based on existing theories about flashing, it could be predicted as shown in Fig. 1 that flashing bubble will form inside crack once the static pressure under evaporation

pressure at this adiabatic system. Leakage rate will be affected significantly by the flashing degree inside crack.

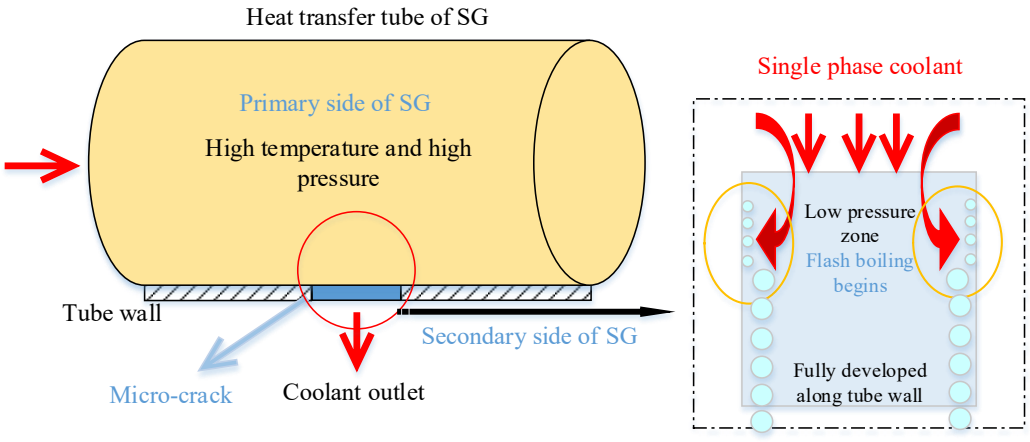

Figure 1. Flash boiling process in micro-crack of a SG heat transfer tube.

A number of theoretical and experimental researches have been carried out on LBB with consideration of flashing process [1-5]. Basically, there are four kinds of semi-empirical two-phase flow models including homogeneous equilibrium, homogeneous non-equilibrium, non-homogeneous equilibrium and non-homogeneous non-equilibrium model, which have been widely used for LBB calculation[6]. A transcendental expression for critical flow rate through convergent passages was built by Henry and Fauske, which is a function of critical pressure ratio [7]. A theoretical and experimental study [2] on the LBB criterion for SG tubes was carried out for various crack leakage in SG. Several criteria [8] for instability of different defects were deduced through leakage rate evaluation and analysis. PICEP (Pipe Crack Evaluation Program) code [9], which was developed by EPRI for the LBB analysis, can calculate both leakage rates and critical crack length for SG tubes [10]. A high accuracy Mathcad code for leakage calculation of PWRs was developed based on a modified Fauske model, where the friction effect was ignored but non-equilibrium effect was considered [11]. The LBB phenomenon in nuclear power plants is researched with code ABAQUS and PIECP by Choon-Yeol et al. [12]. Both codes can provide deformation of the circumferential crack opening area, and the later code could predict the leakage rate with a better accuracy. Both experimental and theoretical analysis on flow and thermal characteristics of the two-phase leakage through micro-crack on pipes are researched by Zhang [13], and several correlations are developed for the prediction of micro-crack leakage rates when coolant flows through narrow and short passages. A leakage analysis code LEABLE [14] is developed for various LBB conditions which covering both single-phase and two-phase leakage flows. The two-phase flow rate is based on an updated Henry-Fauske model by fixing the flashing inception. Its results have a higher precision than those from classic LBB codes including PICEP[9] and

SQUIRT[15]. In addition, a thermal-hydraulic code to calculate critical flow rate of high temperature and high pressure fluid called LEAPOR have also been developed by ORNL(Oak Ridge National Labortory)[16]. In summary, although the classic Henry-Fauske model and its improved modifications have been widely used for LBB simulation, their applications are limited to conditions when the size of crack is large enough satisfying L/D>12 (L and D denote crack the passage length and hydraulic diameter of crack).

The limited application range of the semi-empirical models for LBB calculation prevent them from giving accurate mass flow rates and detailed flow field in short and micro channels. Alternatively, the CFD method has been developed rapidly and widely used for numerical simulation of flashing flows in different configurations especially nozzles in these years [17-21]. It can not only save experimental efforts but also give detailed 3D distribution of thermal hydraulic parameters when coolant flows through the nozzle, orifice or small crack in pressurized pipelines. Generally, there are two approaches for CFD flashing simulation regarding phase change modelling, namely, the cavitation method and evaporation-condensation (or thermal phase change) method. The Rayleigh-Plesset [22, 23] model, which is widely used to describe the growth of single bubble, provides theoretical foundation for the cavitation method, while the evaporation-condensation method is based on interphase heat transfer. Another type of thermal non-equilibrium model, the so-called relaxation model, was built by Schmidt et al. [24] for flash-boiling atomization. Recently, a comprehensive review on description of the flashing phenomenon and existing flow and heat transfer models has been conducted by Liao et al [25-27]. They performed CFD studies on flashing flows in a converging-diverging nozzle, natural circulation loop as well as other scenarios in nuclear applications based on CFX. A main conclusion was that the evaporation-condensation model in the frame of a two-fluid model is superior to the cavitation type model. The transient flashing flow when coolant leak from the main feed water line of SG has been researched by Jo et al. [28] using 3D transient CFD method in CFX. The evaporation-condensation model is used for simulating the phase change process. Chima et al. [29] have calculated the choking flow rate for a fan unit on the basis of 3D Navier-Stokes simulation code SWIFT. The results showed that the rotor choked at the measured flow rate with a normal shock in the passage. A multi-scale CFD approach is used to simulate the choking and flow-regime by Wang et al [30]. CFD-based numerical analyses of choking flashing flow with R134a in a converging-diverging nozzle is conducted by Geng et al [31] with the evaporation and condensation method.

In case of SG tube rupture accidents, the coolant loss rate is determined by the critical two-phase flow process in thin cracks. It represents still a challenge for existing theoretical models to predict the highly non-equilibrium phase change process in such small and short cracks. Mechanism of transient two-phase critical flow in a micro-crack has been insufficiently investigated. In this work, an Euler-Euler phase change model is built for thermal non-equilibrium flashing phenomenon in a short and micro cracked channel. Based on this flashing model, two-phase critical flow in a SG heat transfer tube is reproduced by changing the

backpressure. Three dimensional two-phase thermal hydraulic fields obtained in this research give a brief but clear explanation for the critical flow mechanism. The results about leakage rate are beneficial for the design, maintenance, life extension of SG, and provide thermal hydraulic conditions for the safety analysis of nuclear power system in such a situation.

2. Mathematical models

Both cavitation and evaporation-condensation processes are considered for the modelling of flashing leakage flow through micro-crack. These two models are implemented in combination with two kinds of two-phase models, i.e. the Euler-Euler two-fluid model and a simplified mixture model (see Fig. 2). Finally, five solving schemes or model combinations are built. The liquid phase is assumed as incompressible fluid due to high local sound speed (~1500m/s) and low Mach number ($Ma < 0.3$). The vapor phase is assumed as ideal gas to account for its compressibility under high pressure.

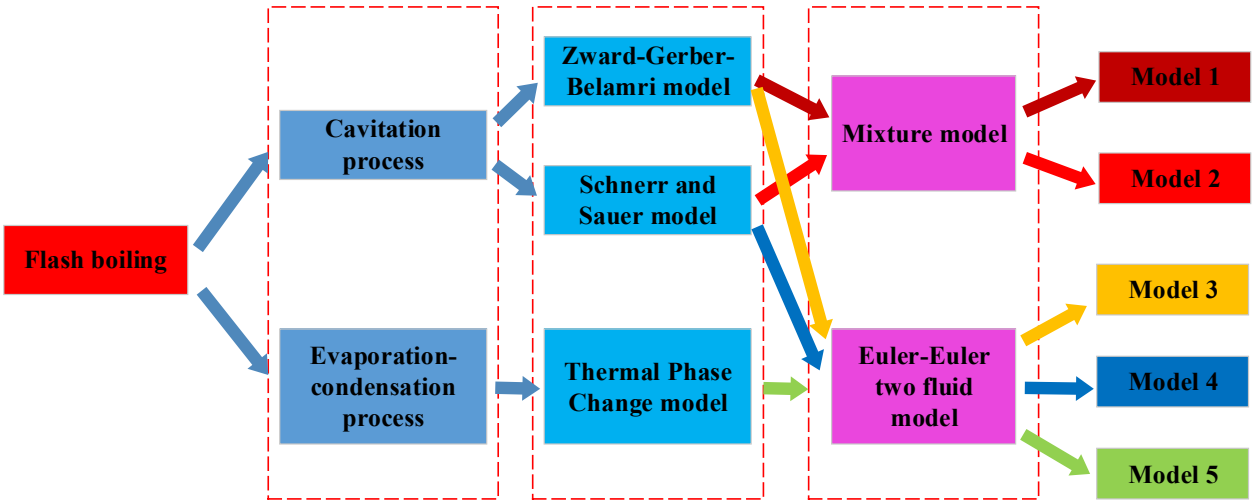

Figure 2. CFD simulation schemes for flash boiling.

For the sake of completeness, all mathematical models used in this research are summarized in this section. Since the Euler-Euler two-fluid model and the simplified mixture model are the basement of all simulation, their conservation equations are presented firstly. Mathematical description of the two phase change mechanisms, i.e. cavitation and evaporation-condensation, are introduced comparatively.

2.1 Conservation equations

2.1.1 Euler-Euler two-fluid model

Regarding the liquid phase as continuum and the gaseous phase as dispersed bubbles, the ensemble-averaged mass, momentum and energy transport equations for phase q read:

Conservation of mass:

$$\frac{\partial}{\partial t}\left(\alpha_q \rho_q\right)+\nabla\cdot\left(\alpha_q \rho_q \vec{v}_q\right)=m_{pq}{}^{+}-m_{qp}{}^{+}\ . \tag{1}$$

Conservation of momentum:

$$\begin{aligned}&\frac{\partial}{\partial t}\left(\alpha_q \rho_q \vec{v}_q\right)+\nabla\cdot\left(\alpha_q \rho_q \vec{v}_q \vec{v}_q\right)=-\alpha_q \nabla P+\nabla\cdot\overline{\overline{\tau}}_q\\&+\left(K_{pq}(\vec{v}_p-\vec{v}_q)+m_{pq}{}^{+}\vec{v}_p-m_{qp}{}^{+}\vec{v}_q\right)+\left(\vec{F}_{lift,q}+\vec{F}_{wl,q}+\vec{F}_{vm,q}+\vec{F}_{td,q}\right)\end{aligned}\ . \tag{2}$$

Conservation of energy:

$$\begin{aligned}&\frac{\partial}{\partial t}\left(\alpha_q \rho_q H_q\right)+\nabla\cdot\left(\alpha_q \rho_q \vec{v}_q H_q\right)=-\alpha_q \frac{dP_q}{dt}+\overline{\overline{\tau}}_q(\nabla\cdot\vec{v}_q)\\&+\left(q_{iq}+m_{pq}{}^{+}H_{qi}-m_{qp}{}^{+}H_{pi}\right)\end{aligned}\ . \tag{3}$$

Wherein the subscript q represents one common phase in the two-fluid model, and p for the other phase. The explanation and units of variables in this section are summarized in the nomenclature table. The terms at the right hand of Eq. (1) denote the mass transfer between the phases p and q, where $m_{pq}{}^{+}$ and $m_{qp}{}^{+}$ represent the positive mass flow rate per unit volume from phase p to phase q and from phase q to phase p, respectively, i.e. $m_{pq}{}^{+}=\max(m_{pq},0)$ and $m_{qp}{}^{+}=\max(m_{qp},0)$. The drag force, lift force, virtual mass force, turbulent dispersion force, wall lubrication force are all considered in the momentum conservation as shown in Eq. (2). The effect of turbulence is included in the stress-strain tensor term, which is solved by a two equation turbulence model and bubble-induced effects are neglected. More details will be given below. q_{iq} is the heat transfer between the interface and the phase q. H_{qi} and H_{pi} represent the interfacial enthalpy carried into and out of the phases. For outgoing phases, they equal to the enthalpy of the phase, while for incoming phases they are set to the saturation enthalpy of the phase.

2.1.2 Homogeneous mixture model

The mixture model is a simplified version of the Euler-Euler two-fluid model with following assumptions.

(a) A homogenous phase is defined to represent the mixture of the two phases.

(b) The momentum interaction between two phases is negligible.

The properties of the mixture phase are defined as in Eq. (4).

$$\begin{aligned}&\rho_m=\alpha_v \rho_v+\left(1-\alpha_v\right)\rho_l\\&\vec{v}_m=\frac{\alpha_v \rho_v \vec{v_v}+\left(1-\alpha_v\right)\rho_l \vec{v_l}}{\rho_m}\\&\mu_m=\alpha_v \mu_v+\left(1-\alpha_v\right)\mu_l\end{aligned} \tag{4}$$

Based on the assumptions, the full Euler-Euler two-fluid model is simplified to following form.

Conservation of mass:

$$\frac{\partial \rho_m}{\partial t} + \nabla \cdot \left(\rho_m \overrightarrow{v_m} \right) = 0 \tag{5}$$

Conservation of momentum:

$$\frac{\partial}{\partial t}\left(\rho_m \overrightarrow{v_m} \right) + \nabla \cdot \left(\rho_m \overrightarrow{v_m} \overrightarrow{v_m} \right) = -\nabla P + \nabla \bullet \left[\mu_m \left(\nabla \overrightarrow{v_m} + \overrightarrow{v_m}^T \right) \right] \tag{6}$$

Conservation of energy:

$$\begin{aligned} \frac{\partial}{\partial t} \sum_{k=1}^{2} \left(\rho_k H_k \right) + \nabla \cdot \sum_{k=1}^{2} \left(\overrightarrow{v_k} \left(\rho_k H_k + P \right) \right) \\ = \nabla \cdot \left(k_{eff} \nabla T \right) \end{aligned} \tag{7}$$

Vapor transport equation:

$$\frac{\partial}{\partial t}\left(\alpha_v \rho_v \right) + \nabla \bullet \left(\alpha_v \rho_v \vec{v}_m \right) = m_{lv} - m_{vl} \tag{8}$$

As we can see, the six-equation model is simplified into a four-equation model where slip velocity is also neglected in this research. In Eq. (7) $k_{eff} = k_v \alpha_v + k_l (1 - \alpha_l)$ denotes an effective thermal conductivity coefficient. There have no heat flux or energy source imported into the flash boiling system, so the interphase mass transfer and the corresponding energy are the main solution goals. Mass transfer between phases is obtained by either a cavitation model or an evaporation-condensation model. In the mixture model, the vapor phase is assumed saturated during the heat and mass transfer process. In the two fluid model, both sides of heat transfer, i.e. the transfer between interface and liquid phase and vapor phase, are all considered.

2.2 Cavitation model

In this model, a number of nucleation sites (micro-bubbles) on saturation pressure corresponding to the liquid temperature is assumed pre-existing and distributed evenly in the narrow channel. Once the pressure drops below the vapor pressure, these micro-bubbles will start to grow according to the Rayleigh-Plesset equation, otherwise, they will collapse.

As we can see, to solve the Eq. (1) and Eq. (8), a constitutive model is needed for the description of mass transfer process. In these two equations, terms m_{pq}^{+}, m_{qp}^{+} and m_{lv}, m_{vl} represent the mass transfer source connected to growth or collapse of flash bubbles which correspond to evaporation and condensation process

respectively. According to the cavitation model the mass transfer source between two phases is determined by the difference of local liquid pressure and evaporation pressure. The cavitation models from Zward-Gerber-Belamri[32] and Schnerr and Sauer[33] behave well regarding both accuracy of results and the stability of simulation.

The mass transfer source in Zward-Gerber-Belamri model is given by:

$$\begin{aligned} m_{lv} &= F_{vap}\frac{3\alpha_{nuc}\left(1-\alpha_v\right)\rho_v}{R_b}\sqrt{\frac{2}{3}\frac{P_v-P}{\rho_l}} \qquad \text{if} \quad P_v \geq P \\ m_{vl} &= F_{cond}\frac{3\alpha_v\rho_v}{R_b}\sqrt{\frac{2}{3}\frac{P-P_v}{\rho_l}} \qquad \text{if} \quad P_v < P \end{aligned} \tag{9}$$

Here P_v denotes the vapor pressure and P the local pressure of liquid phase the parameter. α_{nuc} denotes the nucleation site volume fraction in this model which is set before the simulation. R_b is the nuclei or bubble radius, also prescribed.

While these two terms in the Schnerr and Sauer model are expressed as follows:

$$\begin{aligned} m_{lv} &= F_{vap}\frac{\rho_l}{\rho_m}\frac{3\alpha_v\left(1-\alpha_v\right)\rho_v}{R_b}\sqrt{\frac{2}{3}\frac{\left(P_v-P\right)}{\rho_l}} \qquad \text{if} \quad P_v \geq P \\ m_{vl} &= F_{cond}\frac{\rho_l}{\rho_m}\frac{3\alpha_v\left(1-\alpha_v\right)\rho_v}{R_b}\sqrt{\frac{2}{3}\frac{\left(P-P_v\right)}{\rho_l}} \qquad \text{if} \quad P_v < P \end{aligned} \tag{10}$$

One can see that the source terms are related only to the prescribed R_b value in addition to the two pre-factors.

2.3 Evaporation-condensation model

The evaporation-condensation model in Fluent, also referred to as thermal phase change model in other codes, describes the phase change induced by interphase heat transfer. Once the saturation temperature decreases below the liquid temperature, liquid becomes superheated. At certain degree of superheat it changes into vapor accompanied with energy transfer between the interface and the two phases. The mass transfer source term is obtained from the energy balance at the liquid-vapor interface. The total energy transferred from the interface to the liquid and to the vapor is computed by

$$\begin{aligned} Q_q &= q_{iq} - m_{qp}H_{qi} = h_q A_i\left(T_i - T_q\right) - m_{qp}H_{qi} \\ Q_p &= q_{ip} + m_{qp}H_{pi} = h_p A_i\left(T_i - T_p\right) + m_{qp}H_{pi} \end{aligned} \tag{11}$$

Where h_p and h_q denotes interfacial heat transfer coefficient on the liquid and vapor side, respectively, and T_i is the interfacial temperature. The mass transfer source is obtained directly from Eq. (11) according to heat balance, i.e. $Q_p + Q_q = 0$. The mass transfer through evaporation from the phase q to phase p is:

$$m_{qp} = \frac{h_p A_i \left(T_i - T_p\right) + h_q A_i \left(T_i - T_q\right)}{H_{pi} - H_{qi}} \tag{12}$$

In the current work the interfacial temperature is assumed to be equal to the saturation temperature.

2.4 Constitutive models

A large number of constitutive models are available for the closure of above equations, i.e. closing the Reynolds stress and momentum interaction terms. The selection of appropriate closures refers to the baseline model concept proposed recently by Liao et al. [34,35], which has been applied in the simulation of various flashing flows by the authors, e.g. [19, 36].

2.4.1 Interfacial area density model

It is known that the interfacial area density plays an important role in determining interphase transfer rates. As bubble deformation is neglected instead a spherical shape is assumed, the interfacial area density could be computed as follows:

$$A_i = \frac{6\alpha_q}{d_b} \tag{13}$$

2.4.2 Heat transfer coefficient model

For the use of the evaporation-condensation model the heat transfer coefficients on two phases is of vital importance. There have many models been proposed for simulating evaporation and condensation phenomena [36-39]. Liao et al [26] conducted a comprehensive evaluation on them. The model developed by Hughmark [40] for rigid spheres bubbles is selected here considering its wider range of Re_b which fits the flow status in the micro-channel.

$$Nu_q = \begin{cases} 2 + 0.6 Re_b^{1/2} Pr_q^{1/3} & 0 \le Re_b < 776.06 \;\; 0 \le Pr_q < 250 \\ 2 + 0.27 Re_b^{0.62} Pr_q^{1/3} & 776.06 \le Re_b \;\; 0 \le Pr_q < 250 \end{cases} \tag{14}$$

Where Re_b is the bubble Reynolds number basing on the bubble diameter and relative velocity. Nu_q and Pr_q represents the Nusselt and Prandtl number of the phase q, respectively. Although the heat transfer from/to both liquid and gas sides is considered, the contribution on the gas side is found considerably small.

2.4.3 Momentum transfer models

In the Euler-Euler two-fluid approach constitutive equations are required to describe the momentum transfer between the two phases. In this research, drag force, virtual force, wall lubrication force and turbulence dispersion force are all considered.

Drag force

The term $K_{pq}(\vec{v}_p - \vec{v}_q)$ in Eq. (2) represents the interphase exchange effect due to drag. The coefficient K_{pq} is expressed as

$$K_{pq} = \frac{C_D \rho_l A_i \left|\vec{v}_p - \vec{v}_q\right|}{8} \tag{15}$$

In this research, the drag force coefficient C_D is obtained using the correlation proposed by Ishii and Zuber [41].

Virtual mass force

Virtual mass effect occurs in two-phase flows due to the relative velocity and acceleration. This term might be important during the rapid and transient flashing process. The force acting on the phase *p* is given as follows:

$$\vec{F}_{vm} = C_{vm}\alpha_v \rho_l \left(\frac{\partial \vec{v}_q}{\partial t} - \frac{\partial \vec{v}_p}{\partial t} + (\vec{v}_q \cdot \nabla)\vec{v}_q - (\vec{v}_p \cdot \nabla)\vec{v}_p\right) \tag{16}$$

Where the virtual mass force coefficient C_{vm} is set to a typical value 0.5.

Wall lubrication force

The wall force model is used to describe the lateral force due to the presence of a wall, which tends to push all bubbles away from the wall and assure the zero void condition. The force acts in the normal direction of the wall, and has the following form for bubbles:

$$\vec{F}_{wl} = C_{wl}\rho_l \alpha_v \left|\left(\vec{v}_q - \vec{v}_p\right)_{||}\right|^2 \vec{n}_w \tag{17}$$

The correlation for the coefficient C_{wl} proposed by Hosokawa et al. [42] is adopted in this research

$$C_{wl} = \max\left(\frac{7}{\mathrm{Re}_b^{1.9}}, 0.0217Eo\right) \tag{18}$$

Where Eo denotes the Eötvös number.

Lift force

The lift force acting on the phases results from velocity gradients in the mean flow. For the liquid phase it can be concluded into a form as follows:

$$\overrightarrow{F}_{lift} = C_l \rho_l \alpha_v \left(\vec{v}_v - \vec{v}_l\right) \times \left(\nabla \times \vec{v}_l\right) \tag{19}$$

Where the lift force coefficient model of Tomiyama et al. [43] is adopted here.

2.4.4. Turbulence model

The fluid velocity in the crack is very high indicating strong turbulence effects. It has been shown that there is no significant difference between flow in a normal-sized channel and a micro-channel according to Koo's research [44]. The functional SST (Shear Stress Transport) k-ω model has demonstrated great potential in simulating many practical turbulent flows. Comparative studies have shown that the results obtained from the SST k-ω model are more accurate and stable [45], and have been frequently used in simulating jet flow through micro-channels [46]. Thus, the model is chosen for two phase flow in the heat transfer tube and the micro-crack in this work.

Numerical simulation of flashing process in micro-channels is challenging due to high transiency, short duration and phase change. Special attention is paid to numerics, meshing as well as physical properties to ensure good convergence and stability. The high quality hexahedral mesh is built using ICEM CFD firstly. The coupled algorithm in FLUENT is chosen to solve the velocity and pressure fields. Properties of fluid are estimated based on the database of NIST (National Institute of Standards and Technology) for steam and vapor. Parameters for initial and boundary conditions are all taken from the micro crack tests at XJTU (Xi'an Jiaotong University) [47].

3. Geometric models and computational grids

3.1. Test section description

A series of micro-crack leakage tests has been carried out at XJTU. The tests are categorized into micro-crack field because the COD (crack opening degree) is less than 200 μm. A sketch of test section is shown in Fig 3. The cracked heat transfer tube is surrounded by a pressure vessel to ensure constant backpressure during the test. The coolant flows through the crack into the pressure vessel and the leakage rate is finally obtained by a weighting method. There have two kinds of heat transfer tube where the outer diameter is 17.48 mm and 19.05 mm and the thickness of wall is 1.01 mm and 1.09 mm respectively. With several kinds of crack where the COD is less than 200 μm and length of crack no bigger than 15mm. The maximum pressure inside the heat transfer tube and pressure vessel could reach 9.0 MPa which is less than the real pressure in the primary loop of nuclear plants due to limited performance of test facility. It's also the original

motivation of numerical study in this research aiming to predict real leakage rate under real operating conditions. The static temperature of coolant in heat transfer tube is ranging from 300 K to 553 K.

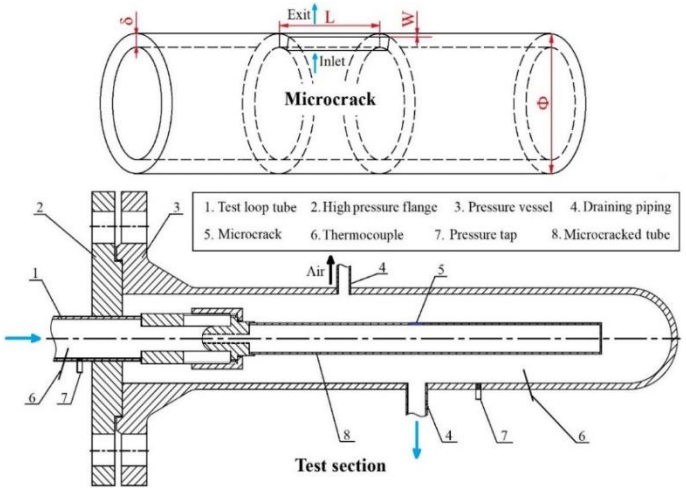

Figure 3. Micro-crack leakage test section.

All of the test sections used in this research are summarized in Table1, where 4 sets of micro-crack test sections are included. Among them, section 1, 2 and 4 are mainly used for research on leakage feature within the micro-crack while section 3 is used for the geometry simplification at the beginning of the simulation. The d_o represents the outer diameter of heat transfer tube, L is the crack length including axial and circumferential directions, W is the COD of crack, δ is crack depth equal to the thickness of tube wall since there have no corner in the cracks.

Table1. Detailed parameters of test sections

No	Morphology	Test section name	d_o (mm)	L (mm)	W (um)	δ (mm)
1	Axial	Φ19.05-LL3-W0.13	19.05	3	130	1.09
2	Axial	Φ19.05-LL3-W0.16	19.05	3	160	1.09
3	Axial	Φ17.48-LL3-W0.13	17.48	3	130	1.01
4	Circumferential	Φ17.48-CL8.3-W0.13	17.48	8.3	130	1.01

The macro and micro appearance of an axial micro-crack in the tests is shown in Fig.4 (a) and Fig.4 (b), respectively. The crack is much smaller compared with the size of heat transfer tube. Since flashing occurs only inside the micro-crack channel and the flow far away has hardly any effect, it is advisable to simulate

a part of the test section instead of the whole. A constant backpressure condition is used to simplify the fluid zone outside of the SG tube.

(a) Test section of heat transfer tubes with an axial micro-crack.

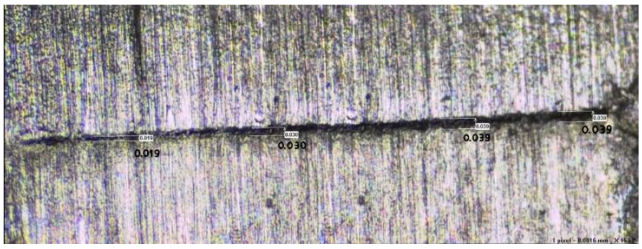

(b) Detailed appearance of an axial micro-crack.

Figure 4. Appearance of micro-crack tubes in SG.

3.2 Geometric model

To evaluate the influence of the length of modelled heat transfer tube, seven geometric models with different entrance and exit lengths have been built, see Fig.5. The stainless steel pipe wall is neglected and adiabatic boundary conditions are applied. The leakage rate predicted with the seven geometric models for one test case is shown in Fig. 6.

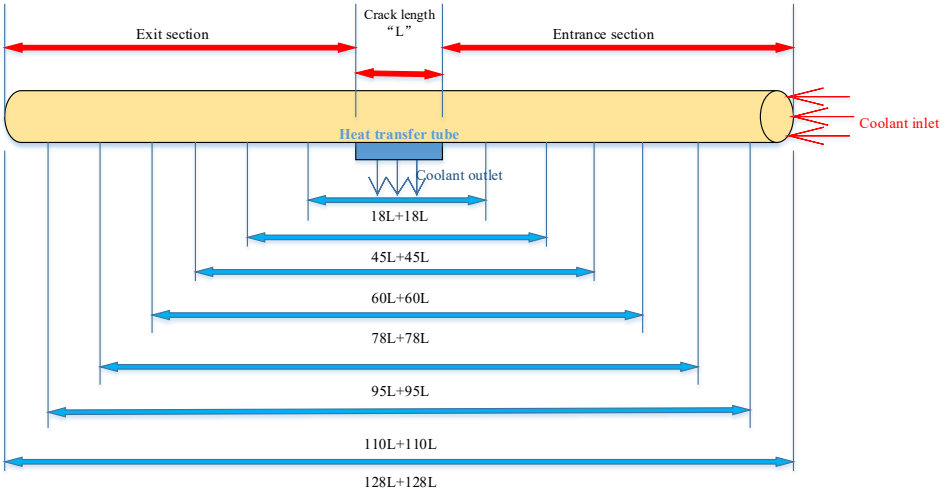

Figure 5. Schematic diagram of seven different geometric models for geometric dependent analysis.

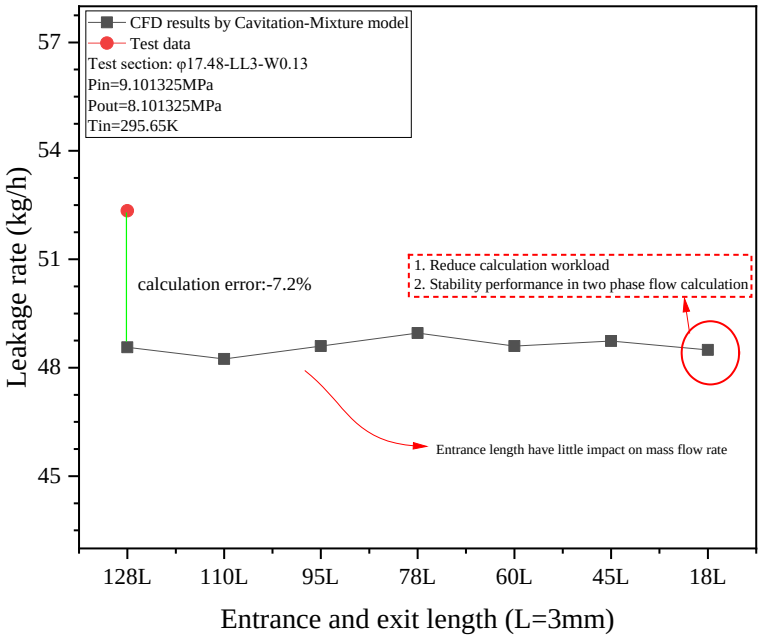

Figure 6. Analysis of effect of entrance and exit length.

The prediction of leakage flow rate remains almost unchanged as the entrance and exit length increases from 18L to 128L. The pre-simulation results show that "18L" is superior to other geometric models because it satisfies the requirement of simulation efficiency, accuracy and stability. All simulations presented in this research are performed on this model.

3.3. Computational grids

Building a high-quality computational grid is important for the simulation of transient and non-equilibrium flashing flows in micro-cracks. The hexahedral structured meshing scheme provided by ICEM CFD is chosen considering that the geometry in this research is rather simple and this strategy could provide higher mesh quality, fewer number of grid cells and better convergence in comparison with unstructured meshing.

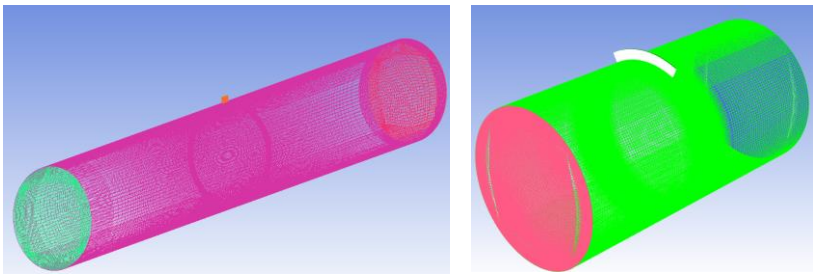

(a) (b)

Figure 7. Meshing model of two kinds of micro-cracks. (a) an axial crack, (b) a circumferential crack.

Two kinds of grids with different crack patterns are shown in Fig. 7. The quality of the meshes well satisfies the requirement of FLUENT. The micro-crack zone is locally refined.

Grid sensitivity analysis needs to be performed before any calculation with the CFD method. Comprehensively, 14 grids with increasing number of cells are built to choose an optimal one for the investigation. It can be seen from Fig. 8 that the leakage flow rate for the crack 3 (see Table 1) remains almost unchanged if the grid amount over 1,000,000. A too coarse grid will lead to obvious over-predictions. Since the micro-crack has little influence on the grid model, the grid with 1,130,000 cells is selected in this research for other test sections with consideration of both simulation accuracy and economy.

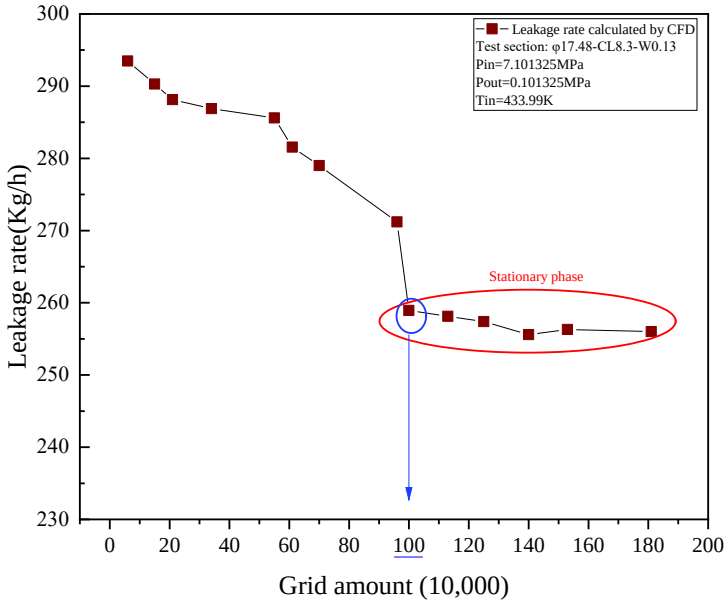

Figure 8. Grid sensitivity analysis.

4. Numerical results

The convergence of all simulations in this research is controlled by monitoring residual curves. The residual threshold for variables are set to be the default value in FLUENT, i.e. 10^{-4}, and the momentum residual in the crack depth direction is found to be the highest one. Both the transient and steady simulations are performed in this research. In the transient cases, the time step is controlled to no more than 0.001s to ensure the stability of simulation.

4.1. Effect of numerical models

As listed in Fig. 2, five different model combinations are built for the simulation of flashing flows based on the available knowledge. A comprehensive comparison between the different approaches is presented in this section aiming at an optimal solution for the micro-crack flashing simulation. The circumferential crack tube φ17.48-CL8.3-W0.13 (No. 4 in Table 1) is chosen for carrying out the comparison simulations. Both

steady and transient calculations have been performed. The distribution of void fraction at the axial and circumferential mid-planes of the micro-channel obtained by different models is shown in Fig. 9. It can be seen that the flashing is started at the upper and lower walls (in the width direction) near the crack inlet position. When the coolant in the heat transfer tube flows through the micro-crack, it experiences a large pressure drop and a region with lower pressure is formed near the wall shortly behind the inlet. In case of Euler-Euler two-fluid model (Model 5), the pre-existing tiny nuclei bubbles are accumulated in the near-wall region under the effect of lift force. These factors facilitate the flashing inception and bubbles appear firstly there. The bubbles continue growing and migrate to the center of the channel downstream. A clear wall-peak void profile is developed in the crack, and the magnitude of the peak reduces gradually due to bubble dispersion in the lateral direction. The circumferential plots in Fig. 9(b) show that the side walls have also an effect on the flashing. The void fraction at the two corners close to the crack exit is clearly higher than that in the middle according to all models due to an abrupt pressure drop.

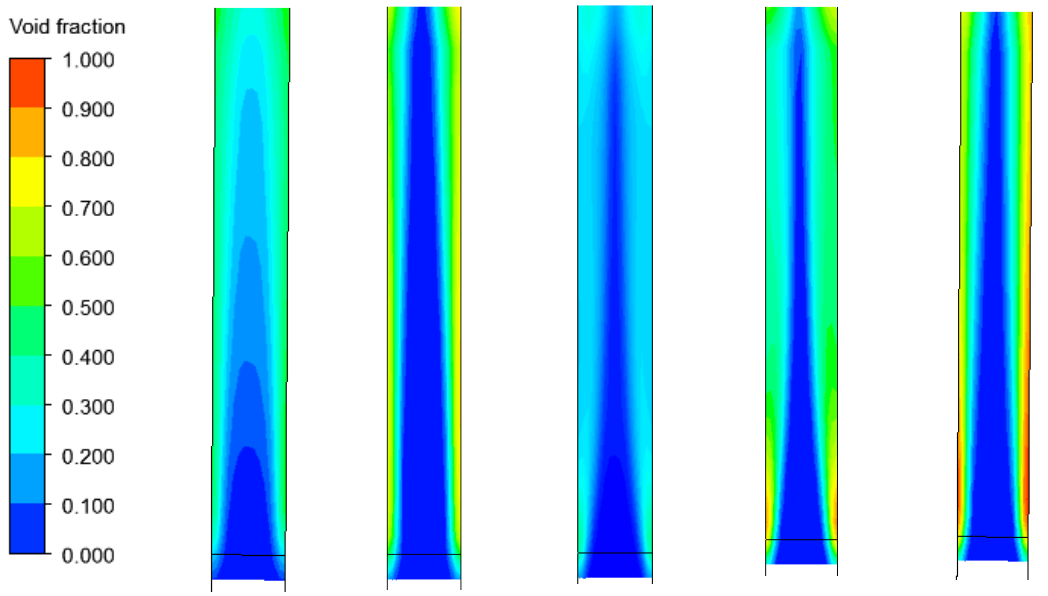

(a) Axial distribution

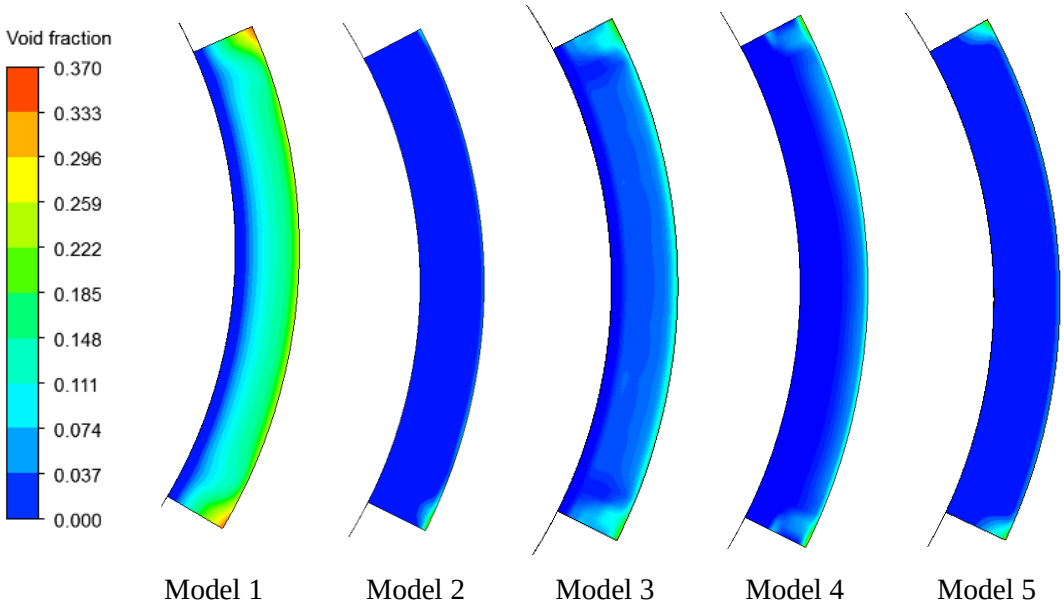

(b) Circumferential distribution

Figure 9. Distribution of void fraction in the micro-crack channel obtained by different models.

Qualitatively similar but quantitatively different void distribution profiles are obtained using the five models. Difference is present not only between the mixture and the two-fluid model (Model 1 vs Model 3, Model 2 vs Model 4), between the cavitation and evaporation-condensation model (Model 3 vs Model 5, Model 4 vs Model 5), but also between the two cavitation models (Model 1 vs Model 2, Model 3 vs Model 4). In general, the evaporation rate predicted by the evaporation-condensation model is larger than that by the cavitation models, and the prediction of the Schnerr and Sauer model is larger than that of the Zwart-Gerber-Belamri model. Furthermore, the two-fluid model tends to suppress the phase change process if it is modelled by a cavitation model. The findings [44, 45] are contradictory to the previous results using the evaporation-condensation model, which showed that the consideration of relative velocity promotes the evaporation process considerably. The cross-section averaged void fraction along the depth of the crack channel is shown in Fig. 10. As one can see, the vapor fraction increases steeply in the regions close to the inlet and outlet because of large local pressure drops.

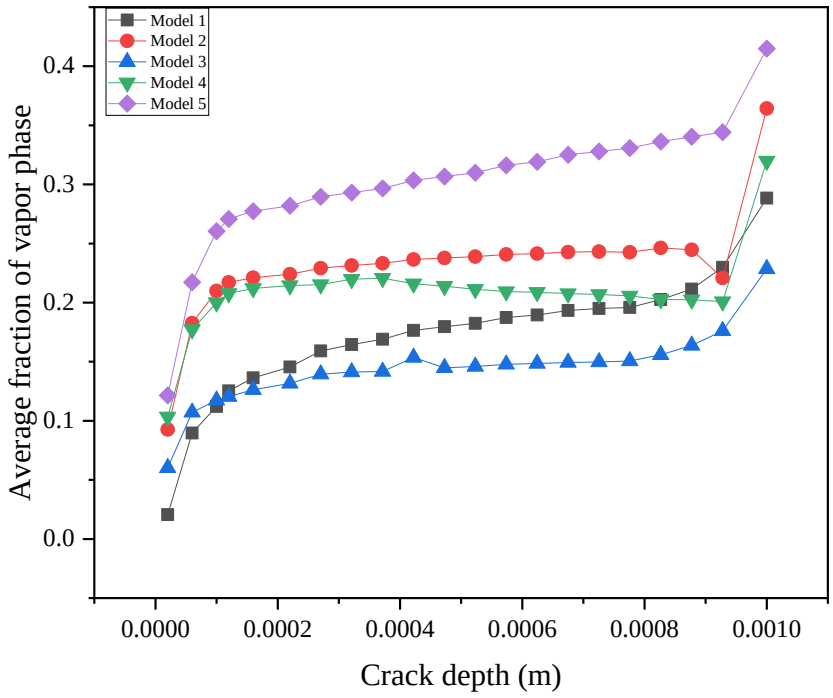

Figure 10. Average void fraction along depth of crack channel.

The leakage rates predicted using the five models as well as their deviation from the measurement are summarized in Table 3. It indicates that all models give an over-prediction of the leakage rate, but the maximal relative error is within 10%. The evaporation-condensation model based on the Euler-Euler method (Model 5) is superior to other solutions and gives the closest prediction. It indicates that thermal effects play an important role under the investigated conditions (high pressure high temperature). The Schnerr and Sauer cavitation model shows a better accuracy than the Zwart-Gerber-Belamri model concerning simulation of flashing and leakage flow through short micro-cracks. The results of leakage rate are consistent overall with the average void fraction presented above. The higher the evaporation rate is lower, the lower leakage rate is higher. However, the prediction of void fraction and leakage rate using Model 2 is both slightly higher than that by Model 4. It may indicate an effect of the void distribution in addition to the average void fraction. From Fig. 9 one can see that the void distribution according to Model 4 is clearly wider to the channel center compared with Model 2.

Table3. Comparison of the predicted and measured leakage rate.

Flashing models	Predicted leakage rate (kg/s)	Measured leakage rate (kg/s)	Relative error (%)
Model 1	256.15	236.30	8.40
Model 2	249.06	236.30	5.40
Model 3	255.44	236.30	8.10
Model 4	247.31	236.30	4.66
Model 5	244.57	236.30	3.50

In conclusion, the CFD method shows a good potential in predicting the micro-crack leakage rate. As shown in Table 3, the calculation accuracy especially the evaporation-condensation model on the basement of Euler-Euler two-phase flow model is much higher than the prediction of existing mature LBB codes such as SQUIRT[15], PICEP[9] and so on where the simulation error could reach 40%. In addition, the detailed 3D information of thermal hydraulic parameters such as phase distribution is useful to discover the leakage mechanism as well as factors that limit the leakage rate from the micro-crack. The evaporation-condensation model based on Euler-Euler method is used to launch the rest simulations with consideration of its higher calculation accuracy and less assumptions.

4.2. Simulation results of Euler-Euler evaporation-condensation model.

Detailed thermal hydraulic parameter distributions are provided to fully understand the flashing process occurring in the micro-crack. In addition to the void fraction in Fig. 9, the steady-state temperature of liquid and vapor is plotted in Fig. 11. Figure 11(a) shows that lower liquid phase temperature occurs in the zones with bubbles. It reflects the thermal phase change results, i.e. the generation and growth of vapor bubbles absorbing heat from the surrounding liquid. In the simulation using the cavitation models, thermal effects are neglected and the liquid temperature remains constant. The highest temperature of vapor phase existing in the inlet area, which could reach 496 K, coincides with the highest pressure inside the heat transfer tube, i.e. before the inlet of the crack channel. The vapor temperature is close to the saturation temperature, and decreases with the pressure along the crack channel, see Fig. 11(b).

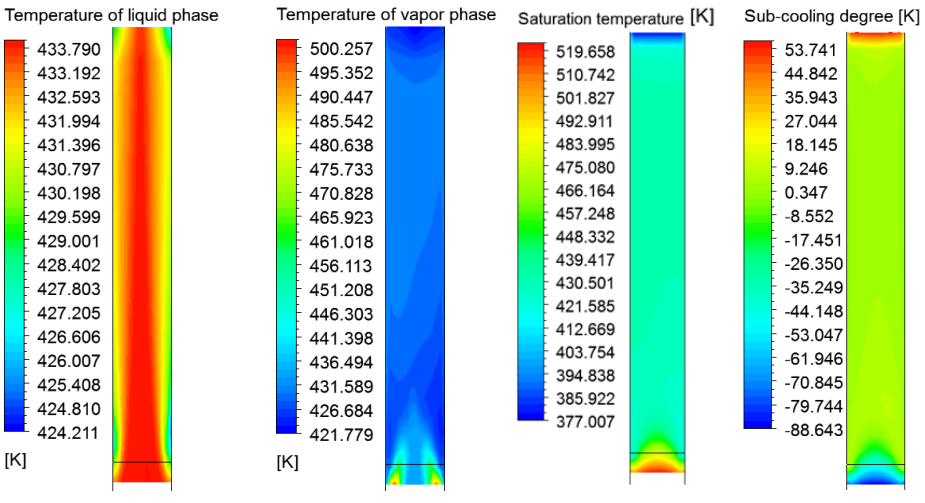

(a) (b) (c) (d)

Figure 11. Temperature field of the two-phase mixture in micro-crack. (a) liquid phase, (b) vapor phase, (c) superheat degree of liquid (d) saturation temperature.

The results in Fig.12 and Fig. 13 reveal the two-phase flow field in micro-crack. The kinetic energy of both phases is bigger at the bubble zone, where a violent phase change process takes place. The highest value exceeds 1000 m^2/s^2.

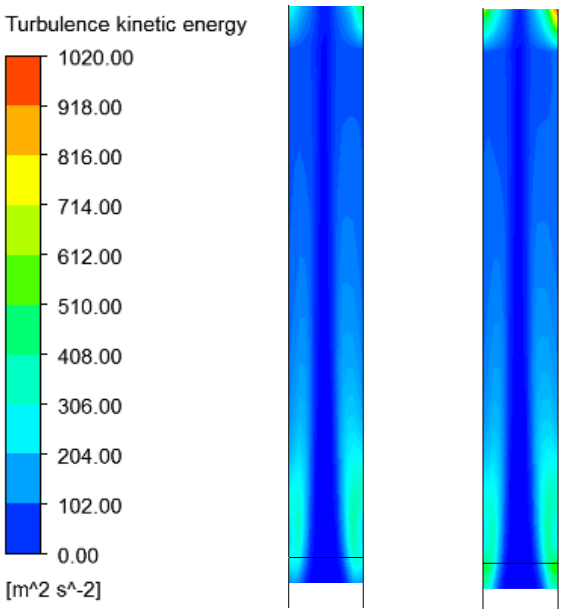

(a) (b)

Figure 12. Turbulence kinetic energy of two phases. (a) liquid phase, (b) vapor phase.

The velocity of both phases behaves similarly with a maximum at the central mainstream zone. The maximum value exceeds 100 m/s. The acceleration of the vapor phase and the velocity difference between the phases near the inlet and outlet are obvious due to large pressure drops. Inside the crack the velocity profiles are relatively flat, and the vapor is decelerated slightly due to the interaction with the liquid phase. In the deceleration region the liquid velocity is higher than the vapor one, and negative relative velocities are observed.

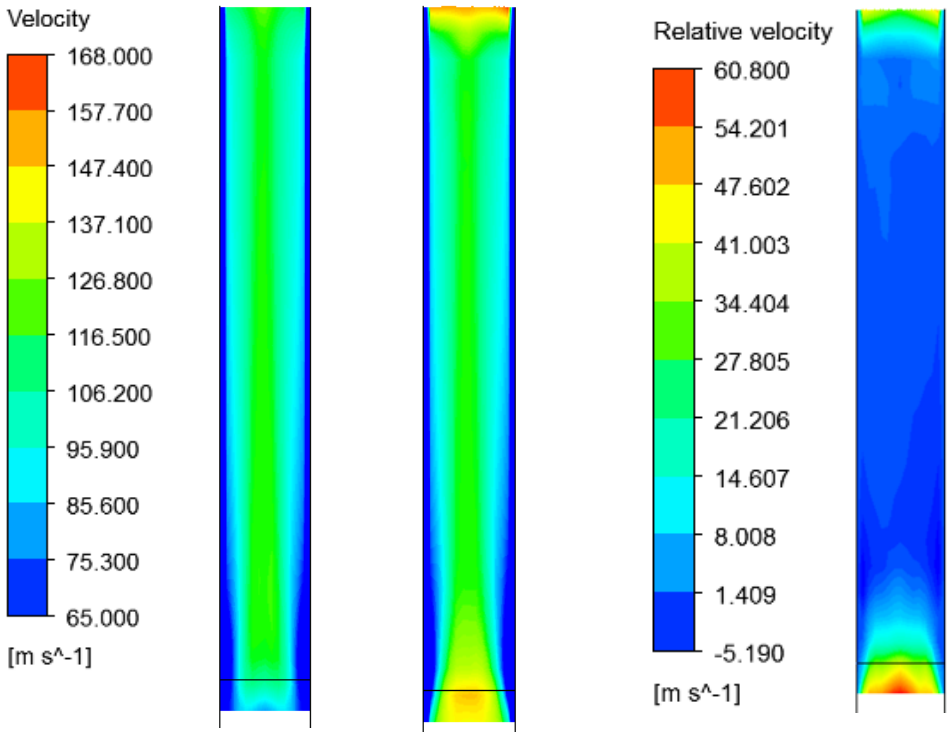

(a) (b) (c)

Figure 13. Velocity distribution. (a) liquid phase, (b) vapor phase, (c) relative velocity.

Finally, the pressure distribution of the mixture phase is presented in Fig. 14. The inlet and outlet pressures are set according to experimental conditions. As discussed above, the pressure drop mainly occurs at the entrance of the crack, which activiates directly the phase change process and the growth of bubbles. The appearance of vapor bubbles helps to recover the pressure so that the pressure remains nearly unchanged along the crack until a significant drop comes again at the exit of the crack. Pressure of coolant decreases rapidly to the backpressure (1 atm in this case) at the outlet position. The regions with lower pressure are consistent with those, where flashing inception and high void fraction are observed (see Fig. 9).

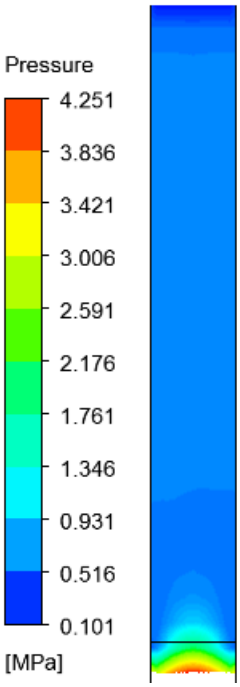

Figure 14. Pressure distribution of mixture phase.

4.3. Comparison with experimental data.

Three sets of micro-crack leakage test data corresponding to the three cracks (No.1, 2, 4) in Table 1 are used to validate the flashing simulation model in this research. Each set consists of a number of test cases, which cover a wide range of coolant temperatures varying from 280 K to 560 K and pressure drops with the inlet pressure changing from 1.101325 MPa to 9.101325 MPa, while the outlet pressure kept at 0.101325MPa. Detailed geometric parameters about test sections are shown in Table 1. As shown in Fig. 15, the predictions of leakage rate provided by the Euler-Euler evaporation-condensation model (Model 5) are in a perfect agreement with the test data of all cases. The leakage rate decreases clearly as the coolant temperature increases. This is because high liquid temperature facilitates the occurrence of flashing, which slows down the leakage process.

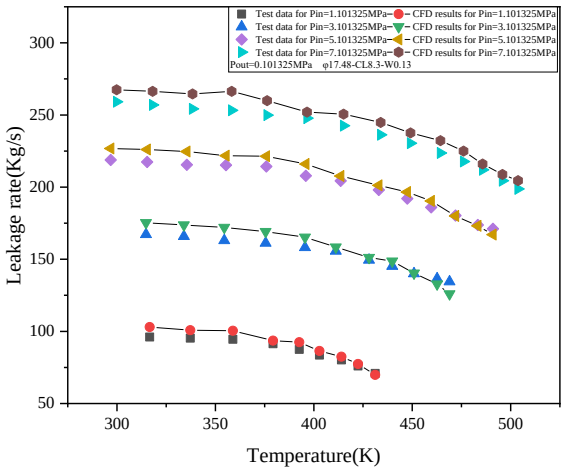

(a)

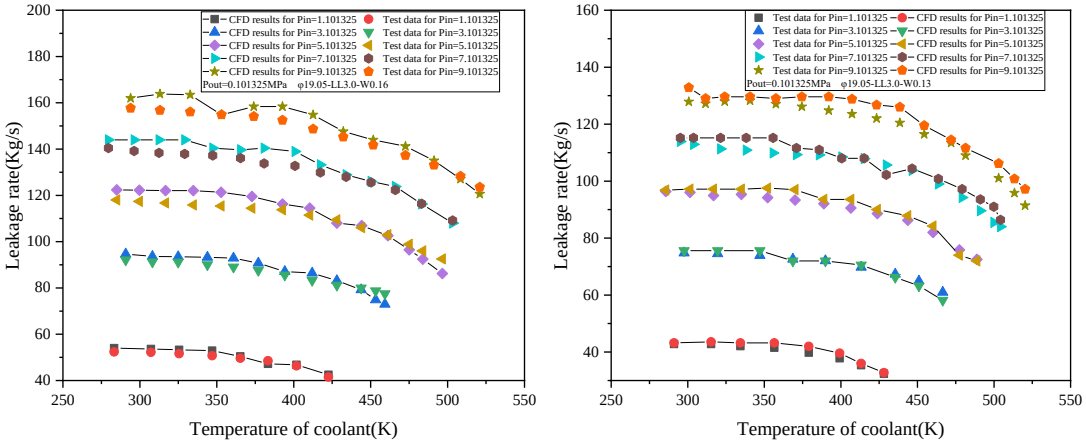

(b) (c)

Figure 15. Comparison between predicted and measured leakage rates ((a) is results comparison of No. 5 test section, (b) is results comparison of No. 2 test section, (c) is results comparison of No. 1 test section. All of CFD results are calculated by Model 5).

The relative error of simulated leakage rates to the data is summarized in Fig.16. It shows an overall over-prediction existing in the cases with temperature lower than 350 K. It may indicate that in these cases the pressure non-equilibrium plays a role in addition to the thermal non-equilibrium. Neglecting of this effect in the current two-fluid model leads to an over-prediction of leakage rates. However, to clarify this point further research is needed. On the other hand, for very high temperature (>500 K) the model behaves clearly different for different cracks in particular for two longitudinal ones, i.e. φ19.05-LL3-W0.13 and φ19.05-LL3-W0.16 (No.1 and No. 2 in Table 1). The leakage rate is over-predicted in crack 1 while under-predicted in crack 2. As shown in Table 1, the unique difference between the two cracks is the width (0.13 mm in crack 1 and 0.16 in crack 2). The reason for inconsistency in the results is not yet clear. Perhaps heat transfer

mechanisms are different in these cases. Nevertheless, the maximal error for all cases in the three test sections is within 8%. It demonstrates that the Euler-Euler evaporation-condensation model has a generally good potential in predicting the micro-crack leakage. The accuracy is even higher than that of widely-used programs (±40~60%) for LBB including PIECP[9] and SQUIRT[15].

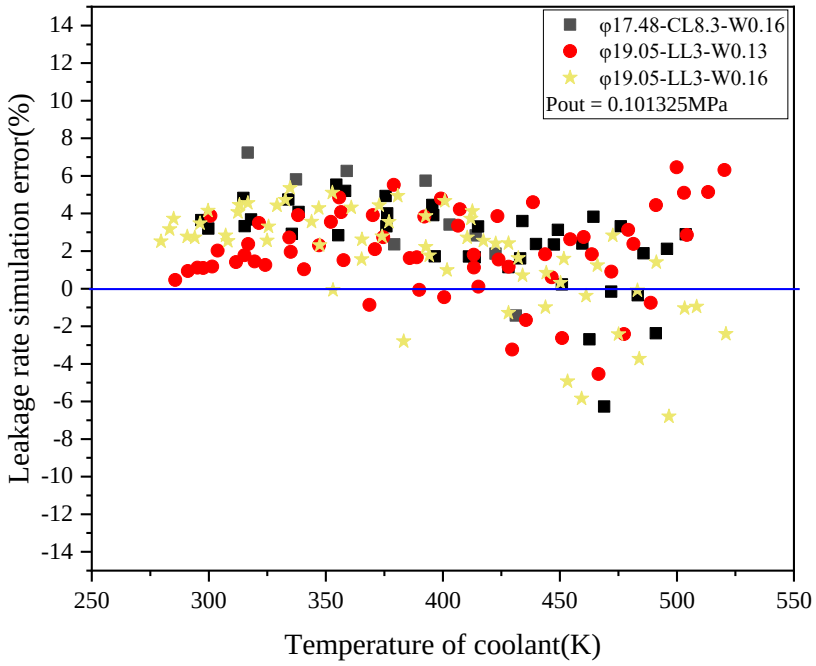

Figure 16. Simulation error distribution by the Euler-Euler evaporation-condensation flashing model.

4.4. Effect of backpressures

The circumferential crack tube φ17.48-CL8.3-W0.13 is selected here for investigating the effect of the backpressure on the leakage rate. The pressure inside the heat transfer tube is 7.101325 MPa and the backpressure varies in the range of 0.101325 ~ 7.0 MPa. The coolant inside the heat transfer tube keeps a hot state with a fixed temperature of 433.99 K, which is realized by using a preheating system during the experiment. Finally, the effect of the backpressure on the leakage rate is investigated by using the cavitation model 4 and evaporation-condensation model 5 on the basis of Euler-Euler two-phase flow model.

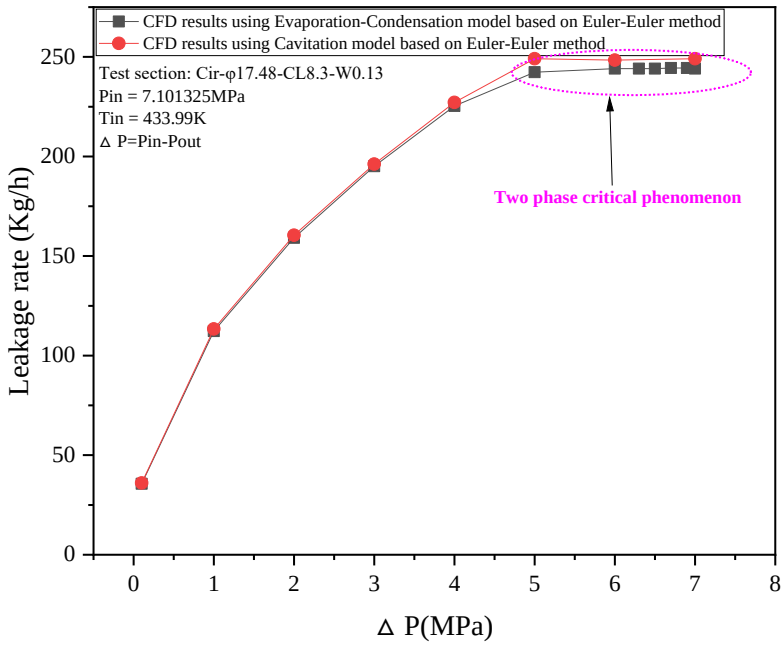

Figure 17. Leakage rate of circumferential shape micro-crack under different backpressures

It can be figured out from Fig.17 that the flash boiling results from two models are quite similar. At high backpressures the two predictions of leakage are quite close. They deviate from each other as the backpressure decreases further. The leakage rate is smaller according to the Euler-Euler evaporation-condensation model. As expected the leakage from the micro-crack increases with the decrease of the backpressure because the evaporation accelerates the flow. However, when the backpressure drops below ca. 2.3 MPa it remains nearly unchanged, which indicates that the critical flow point is reached. In other words, the leakage rate will not be affected by the backpressure if it drops further. The appearance of this phenomenon has been validated by various models in this research. The best accuracy is obtained by the Euler-Euler evaporation-condensation model with comparison to the leakage test data. The results show that the realistic two-phase critical pressure under this condition is between 2.301325 MPa to 2.501325 MPa.

The distribution of pressure and void fraction field at a symmetric cross section of crack under different backpressures are shown in Fig. 18 and Fig. 19, respectively. The results are all loaded from the Euler-Euler evaporation-condensation model. It can be seen from Fig. 18 that the pressure change and local low pressure are affected by the backpressure significantly. The flash boiling phenomenon will disappear when the pressure in the low pressure zone is insufficient to initiate the evaporation. In other words, the lowest saturation temperature at the corresponding pressure is higher than the fluid temperature in the heat transfer tube. Both the pressure near the inlet and outlet sections of the crack increases with the value of backpressure. Figure 19 shows that the flashing is triggered as the backpressure drops to 2.3 MPa. The void fraction in the first half of the crack channel develops to a stable profile, and the local maximum value exceeds 0.97. As

discussed above, the flow reaches the critical condition at this backpressure. It implies that two-phase critical flow occurs when stable flashing process is triggered.

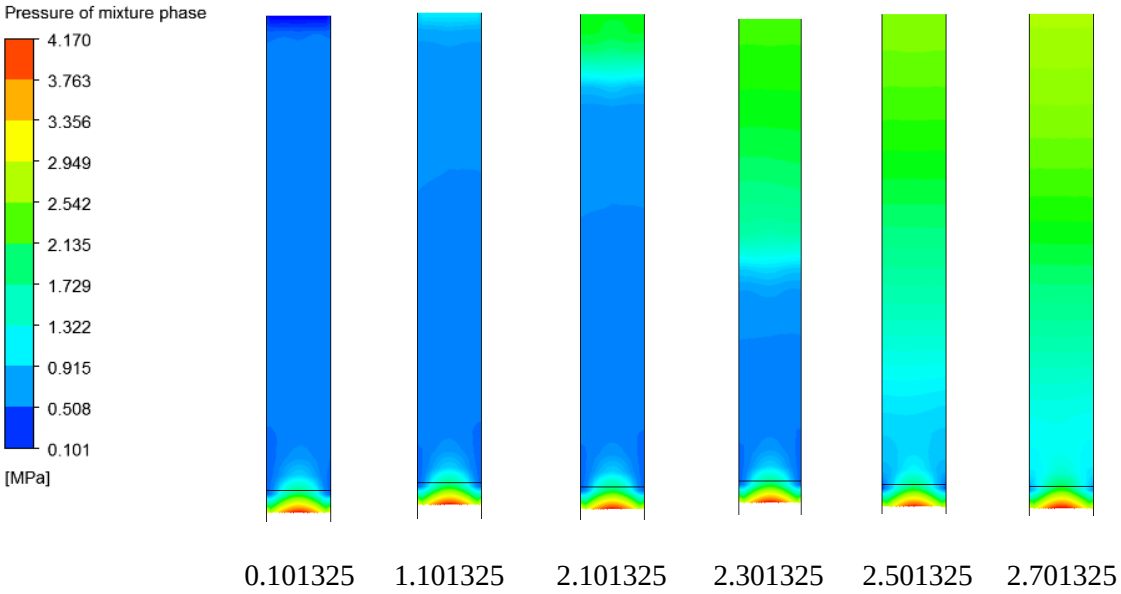

Figure 18. Distribution of pressure at a symmetric section under different backpressure

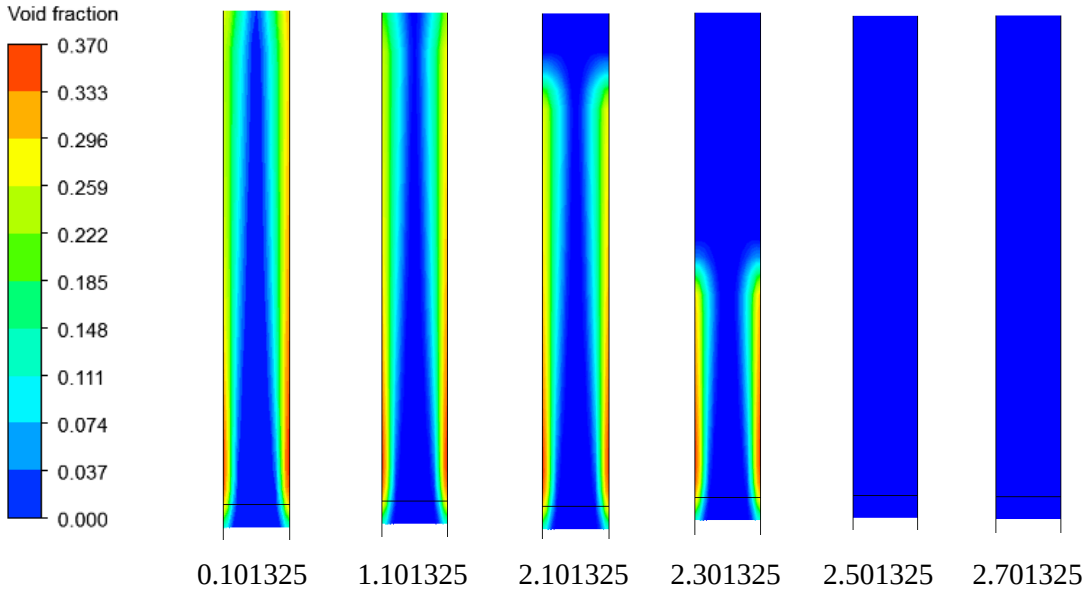

Figure 19. Distribution of void fraction at a symmetric section under different backpressure

According to the theories of the cavitation model and the vaporization-condensation model, flashing bubbles will collapse when the pressure downstream increases above the saturation pressure or correspondingly the saturation temperature exceeds the liquid temperature. The bubble collapse occurs earlier as the backpressure increases, which means the area of flashing zone decreases. There actually have no flashing bubbles when backpressure is greater than the “critical pressure” 2.301325 MPa. It can be figured out from

Fig. 19 that the lower pressure zone near the inlet position of crack is still present but not lower enough to produce bubbles. So only single phase flow prevails in the micro-crack channel.

In summary, the leakage rate increases as the backpressure decreases, because larger driving force (pressure difference or temperature difference) for flashing is obtained. The appearance of many flashing bubbles accelerates the flow through the micro-crack channel, but there exists a limit. The critical pressure is the pressure when flash boiling is stably activated. Further decreases of backpressure will increase the low pressure and flashing zone but will not affect the steady-state critical flow rate.

4.5 Influence of inlet pressure and temperature on critical flow

Based on the results in section 4.4, more calculations under various inlet static pressures are launched for further validation of the two-phase critical model. The circumferential crack tube section φ17.48-CL8.3-W0.13 in Table1 is adopted here as a representative. The leakage rate prediction for all cases is summarized in Fig. 20. The results show that the two-phase critical flow phenomenon in a micro-crack is repeatable under different pressure operations. It can be figured out that the critical pressure is affected significantly by the static pressure in the heat transfer tube of SG. The critical pressure increases with static pressure which means flashing bubble more easily formed under high pressure conditions. The critical pressure could be concluded roughly into a correlation $P_{cr}=0.4P_{in}$, which is consistent with our previous experimental results [47].

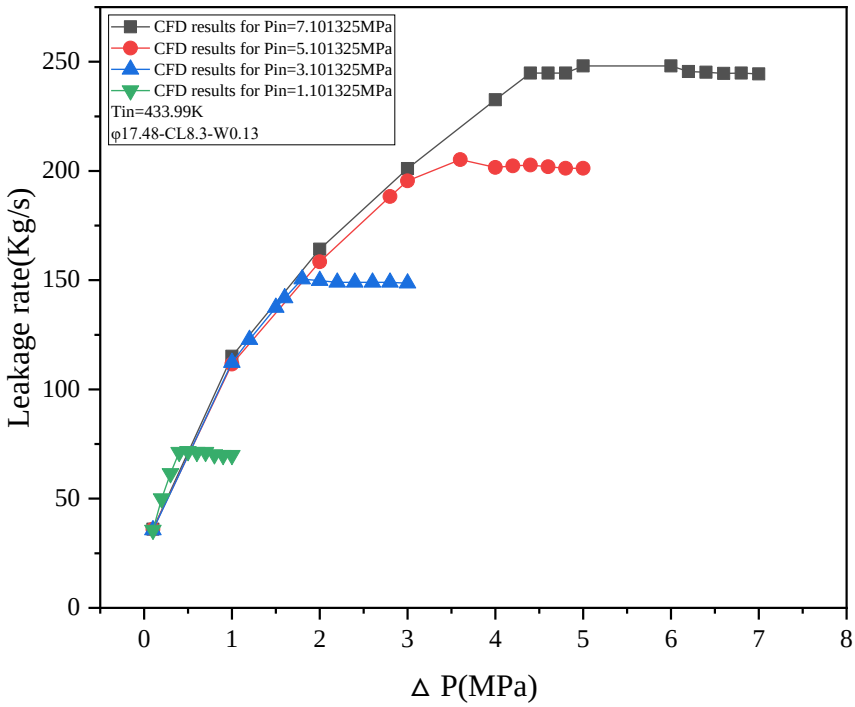

Figure 20. Two-phase critical flow under different inlet static pressures.

To further reveal the effect of static temperature on the flash boiling in the micro-crack, a series of simulations are launched with different temperatures. The predicted leakage rates are plotted in Fig. 21. As expected, hot liquid is apt to evaporate as the pressure drops. The results show that the leakage rate is larger under lower temperature conditions. Under the same inlet pressure, high temperature liquids reach the critical condition earlier as the backpressure decreases. The value of the two-phase critical pressure and leakage rate decreases as the coolant temperature decreases, see Figures 21 and 22.

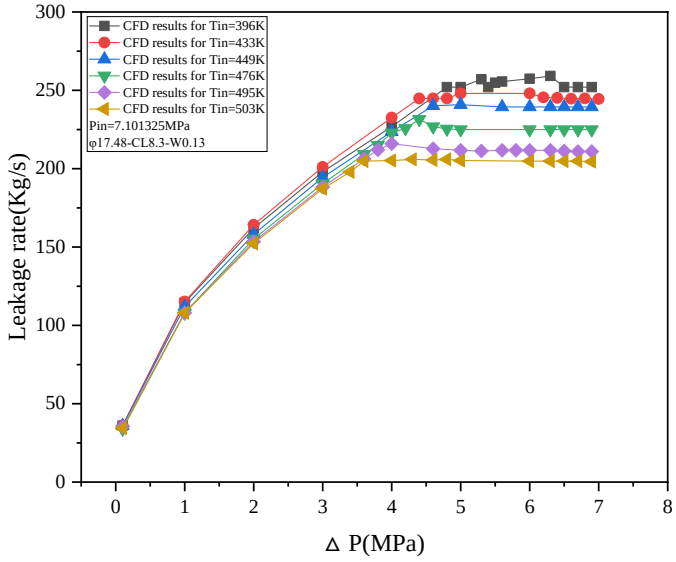

Figure 21. Two-phase critical flow under different static temperatures.

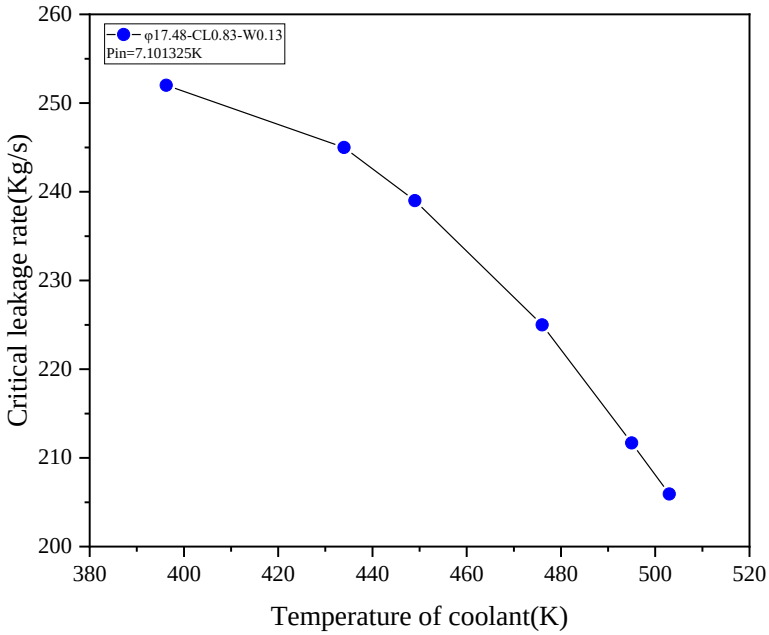

Figure 22. Effect of temperature on critical leakage rate.

5. Conclusion

In this research several typical flashing models are tested for the prediction of micro-crack leakage in a SG heat transfer tube. Two mechanisms including cavitation and evaporation-condensation for the modelling of the phase change process are referred. The phase change models are implemented in the Euler-Euler and the mixture two-phase frameworks, respectively. The evaporation-condensation model with the Euler-Euler method is shown to have the highest accuracy concerning the leakage rate prediction in the micro-crack. The simulation results are validated with the test data obtained by XJTU, which show pretty good agreement. The flash boiling begins at the entrance position of the crack due to large pressure drop, and develops along the crack walls. The flashing process could be well developed and a stable two-phase mixture flows out from the crack once the backpressure is lower enough. On the contrary, the flashing bubbles could not survive and will collapse or the flash boiling cannot be triggered at all once the backpressure is too high. Critical flow phenomenon is observed in the micro-crack if stable flashing occurs. Some conclusions are listed below to give a summary about this research.

1) The evaporation-condensation model incorporated with the Euler-Euler two-fluid approach is more promising in flash boiling simulation of micro-cracks than cavitation models, and its prediction of leakage rates is more close to the data.
2) The leakage simulation results on both circumferential and axial crack-tubes show that lower pressure zones occur behind the inlet and developed along the crack depending on the backpressure. More bubbles are observed at the entrance and exit position of the crack due to large local pressure drop.
3) Two-phase critical flow phenomenon is observed in the micro-crack leakage simulation. Firstly, the leakage rate increases with the pressure driven head over the crack which is achieved by reducing the backpressure. Secondly, flash boiling region increase as the backpressure decreases. However, it is found that the critical flow rate is obtained once the flashing process is triggered stably, and further decrease of the backpressure will not increase the flow rate any more. Both the cavitation and the evaporation-cavitation models can catch this phenomenon, but the prediction of the latter is more close to the measurement.
4) Besides the backpressure, the critical flow rate through the micro-cracks is found to depend on the pressure in the heat transfer tube and initial temperature. Liquid of high pressure and temperature is apt to flash during the depressurization. As a result, the critical leakage rate is lower than low pressure and temperature conditions.

The flash boiling model built in this research could predict the leakage rate with sufficient accuracy, and give three dimensional detailed thermal hydraulic fields for the analysis of the flow in micro-cracks. However, the sensitivity of thermal phase change model on flow conditions is needed to be evaluated further. For example, the effect of pressure non-equilibrium may be non-negligible below a certain temperature

level. The leakage rate prediction results are valuable for monitoring the operation and maintenance of SGs as well as the safety analysis of SG tube rupture accident, e.g. the release of radioactive nuclei from the primary side to the secondary side.

Acknowledgement

This research is supported by Nuclear Thermal-hydraulic Laboratory (XJTU-NuTheL) of Xi'an Jiaotong University and the Institute of Fluid Dynamics at Helmholtz-Zentrum Dresden - Rossendorf. with great thanks to the scholarship provided by graduate school in XJTU and Institute of Fluid Dynamics in HZDR. This research has been supported by National Natural Science Foundation of China Grant NO.12075185.

Reference:

[1] Asada, Y., et al. "Leak-Before-Break verification test and evaluations of crack growth and fracture criterion for carbon steel piping." *International Journal of Pressure Vessels and Piping* 43.1-3 (1990): 379-397.
[2] Flesch, B., and B. Cochet. "Leak-before-break in steam generator tubes." *International Journal of Pressure Vessels and Piping* 43.1-3 (1990): 165-179.
[3] Yin, Songtao, et al. "Mass transfer characteristics of pipeline leak-before-break in a nuclear power station." *Applied Thermal Engineering* 142 (2018): 194-202.
[4] Wang, Mingjun, et al. "Research on the leak-rate characteristics of leak-before-break (LBB) in pressurized water reactor (PWR)." *Applied thermal engineering* 62.1 (2014): 133-140.
[5] Ukadgaonker, Vijay G., and R. Shanmuga Babu. "Review of work related to 'leak-before-break'assessment." *International journal of pressure vessels and piping* 69.2 (1996): 135-148.
[6] Yoon, H. J., M. Ishii, and S. T. Revankar. "Choking flow modeling with mechanical and thermal non-equilibrium." *International journal of heat and mass transfer* 49.1-2 (2006): 171-186.
[7] Henry, Robert E., and Hans K. Fauske. "The two-phase critical flow of one-component mixtures in nozzles, orifices, and short tubes." (1971): 179-187.
[8] Yu, Y. J., et al. "Development of steam generator tube plugging criteria for axial crack." *Fatigue, flaw evaluation and leak-before-break assessments 1994. PVP-Vol. 280*. 1994.
[9] Norris, D., et al. *PICEP: pipe crack evaluation program*. No. EPRI-NP-3596-SR. Electric Power Research Inst., Palo Alto, CA (USA), 1984.
[10] Lang, J. F., et al. "Analysis of leak-before-break for steam generator tubes." *Proceedings of third international topical meeting on reactor thermal hydraulics*. 1985.
[11] Wang, Mingjun, et al. "Research on the leak-rate characteristics of leak-before-break (LBB) in pressurized water reactor (PWR)." *Applied thermal engineering* 62.1 (2014): 133-140.
[12] Lee, Choon-Yeol, et al. "Application of the leak before break (LBB) concept to a heat exchanger in a nuclear power plant." *KSME international journal* 15.1 (2001): 10-20.
[13] Zhang, Jing, et al. "Experimental study on the flow and thermal characteristics of two-phase leakage through micro crack." *Applied Thermal Engineering* 156 (2019): 145-155.
[14] Zhang, Jing, et al. "A code development for leak before break (LBB) leakage from supercritical to subcritical conditions." *Progress in Nuclear Energy* 103 (2018): 217-228.
[15] Paul, D. D., et al. *Evaluation and refinement of leak-rate estimation models. Revision 1*. No. NUREG/CR--5128-REV. 1. Nuclear Regulatory Commission, 1994.
[16] Williams, Paul T., and Shengjun Yin. *Prediction Of The Leakage Rate For Cracked Pipes In Nuclear Power Plants*. Oak Ridge National Lab.(ORNL), Oak Ridge, TN (United States), 2013.
[17] Calay, R. K., and A. E. Holdo. "Modelling the dispersion of flashing jets using CFD." *Journal of hazardous materials* 154.1-3 (2008): 1198-1209.

[18] Janet, Jon Paul, Yixiang Liao, and Dirk Lucas. "Heterogeneous nucleation in CFD simulation of flashing flows in converging–diverging nozzles." *International Journal of Multiphase Flow* 74 (2015): 106-117.
[19] Liao, Yixiang, and Dirk Lucas. "3D CFD simulation of flashing flows in a converging-diverging nozzle." *Nuclear Engineering and Design* 292 (2015): 149-163.
[20] Maksic, S., and D. Mewes. "CFD-calculation of the flashing flow in pipes and nozzles." *Fluids Engineering Division Summer Meeting*. Vol. 36150. 2002.
[21] Marsh, C. A., and A. P. O'Mahony. "Three-dimensional modelling of industrial flashing flows." *Progress in Computational Fluid Dynamics, an International Journal* 9.6-7 (2009): 393-398.
[22] Plesset, M.S. "Bubble dynamics" In *Cavitation in Real Liquids*, ed. R. Davies, Ed., Elsevier Publishing Company, Amsterdam, 1964
[23] Rayleigh, Lord. "VIII. On the pressure developed in a liquid during the collapse of a spherical cavity." *The London, Edinburgh, and Dublin Philosophical Magazine and Journal of Science* 34.200 (1917): 94-98.
[24] Schmidt, David P., S. Gopalakrishnan, and Hrvoje Jasak. "Multi-dimensional simulation of thermal non-equilibrium channel flow." *International journal of multiphase flow* 36.4 (2010): 284-292.
[25] Liao, Yixiang, and Dirk Lucas. "Computational modelling of flash boiling flows: A literature survey." *International Journal of Heat and Mass Transfer* 111 (2017): 246-265.
[26] Liao, Yixiang, and Dirk Lucas. "Evaluation of interfacial heat transfer models for flashing flow with two-fluid CFD." *Fluids* 3.2 (2018): 38.
[27] Liao, Yixiang, and Dirk Lucas. "Possibilities and limitations of CFD simulation for flashing flow scenarios in nuclear applications." *Energies* 10.1 (2017): 139.
[28] Jo, Jong Chull, et al. "Numerical prediction of a flashing flow of saturated water at high pressure." *Nuclear Engineering and Technology* 50.7 (2018): 1173-1183.
[29] Chima, Rodrick, et al. "CFD models of a serpentine inlet, fan, and nozzle." *48th AIAA Aerospace Sciences Meeting Including the New Horizons Forum and Aerospace Exposition*. 2010.
[30] Wang, Wei, Bona Lu, and Jinghai Li. "Choking and flow regime transitions: simulation by a multi-scale CFD approach." *Chemical Engineering Science* 62.3 (2007): 814-819.
[31] Geng, Lihong, Huadong Liu, and Xinli Wei. "CFD analysis of the flashing flow characteristics of subcritical refrigerant R134a through converging-diverging nozzles." *International Journal of Thermal Sciences* 137 (2019): 438-445.
[32] Zwart, Philip J., Andrew G. Gerber, and Thabet Belamri. "A two-phase flow model for predicting cavitation dynamics." *Fifth international conference on multiphase flow, Yokohama, Japan*. Vol. 152. 2004.
[33] Kozubková, Milada, Jana Rautová, and Marian Bojko. "Mathematical model of cavitation and modelling of fluid flow in cone." *Procedia Engineering* 39 (2012): 9-18.
[34] Liao, Yixiang, Eckhard Krepper, and Dirk Lucas. "A baseline closure concept for simulating bubbly flow with phase change: A mechanistic model for interphase heat transfer coefficient." *Nuclear Engineering and Design* 348 (2019): 1-13.
[35] Liao, Yixiang, et al. "Eulerian modelling of turbulent bubbly flow based on a baseline closure concept." *Nuclear Engineering and Design* 337 (2018): 450-459.
[36] Liao, Yixiang, and Dirk Lucas. "Numerical analysis of flashing pipe flow using a population balance approach." International Journal of Heat and Fluid Flow 77 (2019): 299-313.
[37] Chen, Y. M., and F. Mayinger. "Measurement of heat transfer at the phase interface of condensing bubbles." *International journal of multiphase flow* 18.6 (1992): 877-890.
[38] Thome, J. R., V. Dupont, and Anthony M. Jacobi. "Heat transfer model for evaporation in microchannels. Part I: presentation of the model." *International Journal of Heat and Mass Transfer* 47.14-16 (2004): 3375-3385.
[39] Jacobi, Anthony M., and John R. Thome. "Heat transfer model for evaporation of elongated bubble flows in microchannels." *J. Heat Transfer* 124.6 (2002): 1131-1136.
[40] Hughmark, G. A. "Mass and heat transfer from rigid spheres." *AIChE Journal* 13.6 (1967): 1219-1221.

[41] Ishii, Mamoru, and Novak Zuber. "Drag coefficient and relative velocity in bubbly, droplet or particulate flows." *AIChE journal* 25.5 (1979): 843-855.
[42] Hosokawa, Shigeo, et al. "Lateral migration of single bubbles due to the presence of wall." *Fluids Engineering Division Summer Meeting*. Vol. 36150. 2002.
[43] Tomiyama, Akio, et al. "Transverse migration of single bubbles in simple shear flows." *Chemical Engineering Science* 57.11 (2002): 1849-1858.
[44] Koo, Junemo, and Clement Kleinstreuer. "Liquid flow in microchannels: experimental observations and computational analyses of microfluidics effects." *Journal of Micromechanics and Microengineering* 13.5 (2003): 568.
[45] Dang Le, Quang, et al. "Computational fluid dynamics modeling of flashing flow in convergent-divergent nozzle." *Journal of Fluids Engineering* 140.10 (2018).
[46] Th. Frank, J. M. Shi, and A. D. Burns. "Validation of Eulerian Multiphase Flow Models for Nuclear Safety Applications". *Third International Symposium on Two-Phase Flow Modeling and Experimentation*, Pisa, Italy. Sept. 22–24, 2004.
[47] Zhang, K., et al. "Experimental study on leak flow rate characteristics of high pressure subcooled water through axial and circumferential microcracks of steam generator tubes under high back pressure conditions." *Annals of Nuclear Energy* 145 (2020): 107551.